Optimizing BOLD sensitivity in the 7T Human Connectome Project resting-state fMRI protocol using plug-and-play parallel transmission

Vincent Gras [a], Benedikt A. Poser [b], Xiaoping Wu [c], Raphaël Tomi-Tricot [a], Nicolas Boulant [a,*]

[a] NeuroSpin, CEA, University of Paris-Saclay, Gif-sur-Yvette, France
[b] Department of Cognitive Neuroscience, Faculty of Psychology and Neuroscience, Maastricht University, Maastricht, the Netherlands
[c] Center for Magnetic Resonance Research, University of Minnesota, Minneapolis, MN, USA

ARTICLE INFO

ABSTRACT

The Human Connectome Project (HCP) has a 7T component that aims to study the human brain's organization and function with high spatial and temporal resolution fMRI and diffusion-weighted acquisitions. For whole brain applications at 7T, a major weakness however remains the heterogeneity of the radiofrequency transmission field (B_1^+), which prevents from achieving an optimal signal and contrast homogeneously throughout the brain. In this work, we use parallel transmission (pTX) Universal Pulses (UP) to improve the flip angle homogeneity and demonstrate their application to highly accelerated multi-band EPI (MB5 and GRAPPA2, as prescribed in the 7T HCP protocol) sequence, but also to acquire at 7T B_1^+-artefact-free T_1- and T_2-weighted anatomical scans used in the pre-processing pipeline of the HCP protocol. As compared to typical implementations of pTX, the proposed solution is fully operator-independent and allows "plug and play" exploitation of the benefits offered by multi-channel transmission. Validation in five healthy adults shows that the proposed technique achieves a flip angle homogeneity comparable to that of a clinical 3 T system. Compared to standard single-channel transmission, the use of UPs at 7T yielded up to a two-fold increase of the temporal signal-to-noise ratio in the temporal lobes as well as improved detection of functional connectivity in the brain regions most strongly affected by B_1^+ in-homogeneity.

1. Introduction

In functional magnetic resonance imaging (fMRI), there is a growing interest in performing neuro-scientific studies at ultra-high field (UHF) to benefit from the supra-linear increase in the blood oxygenation level dependent (BOLD) signal change with the static magnetic field strength (B_0) (Yacoub et al., 2001). Following this trend, e.g. the original young adult Human Connectome Project (HCP) contains a 7T component that targets functional and diffusion MRI with high spatiotemporal resolutions (Uğurbil et al., 2013; Van Essen et al., 2013) to study the brain's organization and some of its functions. The 7T HCP resting state fMRI (RS-fMRI) protocol comprises a ten-fold accelerated (×5 simultaneous multi-slice and ×2 in-plane acceleration) multi-band echo-planar imaging (MB-EPI, a.k.a. SMS-EPI) acquisition which allows sampling the BOLD signal at 1.6 mm spatial and 1 s temporal resolution.

A major challenge of 7T MRI with large volume coverage is the heterogeneity of the radiofrequency (RF) transmission field (B_1^+) which, if not corrected, would result in nonuniform flip angles and tissue contrast across the whole brain. The RF nonuniformity is due to standing wave effects that become problematic in the head at B_0 of 7T and up, where the RF wavelength becomes comparable to the head size and falls below 13 cm. The consequence of the resulting flip-angle variation in 7T (RS-fMRI) scans such as the ones used in the 7T HCP study is a reduced performance in the detection of BOLD signal mostly in the inferior and temporal brain regions. Similarly affected at 7T are the magnetization prepared rapid gradient echo (MPRAGE) (Mugler and Brookeman, 1990) and 3D variable flip angle turbo spin echo (3D-VFA-TSE, a.k.a. SPACE (Mugler et al., 2000)) acquisitions which are part of the minimal pre-processing pipeline of the HCP protocol (Glasser et al., 2013). The inherent limits of these anatomical scans yet can be compensated by providing 3 T images to complement the 7T fMRI scans (Glasser et al., 2013) but it remains desirable to be able to conduct the entire set of acquisitions at 7T.

In order to mitigate the problem of flip-angle inhomogeneity at UHF, the 7T HCP has adopted a practical approach, which is to place dielectric pads (filled with calcium titanate) around the head near the regions most

---

strongly affected. The high dielectric constant of the padding material ($\varepsilon_r = 100$ or higher) notably affects the properties of the environment 'seen' by the RF waves and, if placed adequately, steers them so as to locally enhance the RF field (Webb, 2011). While effective locally, it appears extremely challenging to achieve homogeneous RF fields over extended regions with the use of dielectric pads alone.

Parallel RF transmission (pTX) technology (Katscher et al., 2003; Zhu, 2004) is one more elaborate approach to improve flip-angle uniformity, and use of this still not wide-spread technology has recently been proposed for whole-brain RS-fMRI acquisition at the same spatiotemporal resolutions as in the 7T HCP (Wu et al., 2019). Specifically, in this work, the MB-EPI sequence (Moeller et al., 2010; Setsompop et al., 2012; Vu et al., 2017) used in HCP was modified to enable slice-specific RF shimming. In doing so, the coefficient of variation (CV), i.e., standard deviation (std)/mean) of the whole brain flip-angle distribution, was ~15% for pTx (with eight independent transmit channels) versus ~24% for conventional single channel transmission (sTX), and ~20% if 3D whole-head RF shimming was performed (Gras et al., 2017a; Krishnamurthy et al., 2019). This proved useful in enhancing the temporal SNR especially in the regions adversely affected by voids in B_1^+. Other studies have also shown the potential of pTX technology to recover optimal signal and contrast across the whole brain at 7T in MPRAGE (Cloos et al., 2012a), diffusion (Wu et al., 2018) as well as 3D TSE (Eggenschwiler et al., 2014; Massire et al., 2015; Beqiri et al., 2018; Gras et al., 2018) acquisitions.

However one drawback of those conventional pTX approaches is that the optimized pTX excitations or refocusing were obtained by subject-specific numerical optimization, performed 'online' (i.e., while the subject was waiting in the scanner), based on subject- and session-specific B_1^+ maps that first had to be acquired in the same session. In practice, this requires an additional B_1^+ calibration scan whose duration amounts to at least 20 s per transmit channel for optimized B_1^+ mapping sequences, and the subsequent numerical optimization of the pTX excitation which can also take up to several minutes.

The concept of Universal Pulse design (Gras et al., 2017b) offers a solution for entirely removing the need for subject- or session-specific field mapping and subsequent on-line optimization of the RF pulses. The benefits of pTX are instead utilized in a fully automated or "plug-and-play" manner, offering more flexibility and reactivity for the operator during the exam. In contrast, full automation starting from subject-based acquired B_1^+ maps and comprising on-line RF pulse tailoring in principle is possible but to date is not available, and would still require extensive developments. Plug-and-play pTX here is done by pre-calculating RF pulses that were optimized on a series of B_1^+ and B_0 offset maps obtained from a representative sample of the adult population. The RF pulse optimization thus takes place separately from the scan session, and consists in minimizing an objective function that maximizes the average performance of the pTX excitation across the database of field maps (Gras et al., 2017a). The result of this procedure is universally valid pulses, hence the term Universal Pulses (UP).

To better cope with inter-subject variability of the B_1^+ profile, UPs are often designed by considering a broader class of pTX excitation modes than RF shimming, namely *dynamic* RF shimming (Padormo et al., 2016). Here, the capabilities of pTX are more fully exploited in that dynamic RF shimming pulses take advantage of the transmit-sense (Katscher et al., 2003) concept to homogenize the flip angle distribution. One potential weakness with such types of excitation yet is the possible increase in the excitation duration as compared to standard RF shimming, with impact on the response of off-resonant spins but which can be taken into account in the pulse optimization (Grissom et al., 2006). The most prominent examples for this are 2D spokes excitation (Saekho et al., 2006; Setsompop et al., 2008) and 3D k_T -points (Cloos et al., 2012b) which apply small "gradient blips" in between a series of selective or non-selective pulses, so as to spatially modulate the flip angle phase of each subpulse and yield an overall more homogeneous flip angle distribution within a

slice or across a volume. Importantly, as shown by Tse and colleagues in recent work at 9.4 T (Tse et al., 2016), the 2D multi-spoke dynamic RF shimming technique can be extended to generate pTX multi-band RF pulses that simultaneously excite multiple slices.

In this work, we report on the design of multi-band Universal Pulses to conduct HCP-style RS-fMRI studies at 7T. As in the original 7T HCP, the RS-fMRI was acquired using a 2D SMS sequence with factor-5 slice acceleration. We also show that a complete shift towards 7T acquisitions is possible, with additional pTX-UP enabled T_1 - and T_2 -weighted anatomical scans that can be incorporated in the preprocessing pipeline. The excitation pulse of the MB-EPI sequence was replaced by bipolar two-spoke (MB-5) UPs, the non-selective square pulses of the SPACE acquisition by a scalable (Eggenschwiler et al., 2014; Gras et al., 2018) 9-k_T UP, the adiabatic inversion preparation pulse of the MPRAGE sequence by a 9-k_T inversion UP, and the small FA square pulse of the FLASH readout module of the MPRAGE sequence by a 7-k_T UP. This pTX-UP implementation of the RS-fMRI protocol is compared experimentally on five healthy adults with the same protocol played with standard pulses and single channel transmission (sTX), without and with dielectric pads. Using retrospective flip angle simulations based on measured suject-specific B_1^+ maps, the benefit of the UP integration into the RS-fMRI protocol in terms of signal homogeneity is compared with subject and slice specific RF shimming strategies. Temporal SNR (tSNR) is quantified based on the measured EPI time-series of each volunteer. A seed-based analysis of the default mode network (DMN) is also reported to evaluate the gain in terms of functional connectivity estimation.

2. Material and methods

All experiments were performed on a 7T S Magnetom MRI system (Siemens Healthineers, Erlangen, Germany, software baseline VB17A and step 2.3 pTX) equipped with an eight-channel pTX system (1 kW per channel), and SC72 body gradient coil (nominal slew rate 200 mT/m/ms and 40 mT/m maximum amplitude). The vendor-provided head-coils were used: 8Tx-32Rx for pTX acquisitions, 1Tx-32Rx for the sTx reference experiments (both from Nova Medical, Wilmington, MA, USA). The implementation of the HCP resting-state fMRI protocol used custom MB-EPI, MPRAGE and SPACE sequences to enable pTX and UPs integration. Measurements were performed on 5 healthy adult subjects (2 women) and were divided for each one of them into three 1-h sessions, run on different days, to cover the pTX and the sTX operation modes with and without dielectric padding. The dielectric pads were based on a calcium titanate ($CaTiO_3$) suspension (Webb, 2011) and were 0.5 cm thick and 10 cm long (square form). Two such pads were placed against the subjects ears. For the acquisition in sTX, the standard RF transmitter adjustment procedure provided by the scanner's manufacturer was used. In pTX, this calibration step was disabled and the transmitter adjustment was specified by the UPs used in the respective sequences, as detailed below. Adherence to the SAR guidelines was ensured by real-time SAR supervision using a Virtual Observation Point (VOP) model (Eichfelder and Gebhardt, 2011) of the SAR distribution in the head that was implemented using home-made routines and electromagnetic simulations provided by the coil vendor. After experimental phantom validation on the scanner, the VOPs were augmented by safety factors to account for RF coil modelling imperfections, inter-subject variability in the peak SAR value (Garrec et al., 2016; Boulant et al., 2018) and uncertainties in the directional coupler measurements of the TX Array system (Gumbrecht, 2013), resulting in a total safety factor of 2.3 (Boulant et al., 2018). The study was approved by the local ethics committee and all volunteers gave written informed consent.

2.1. MRI protocol

The MRI acquisition consisted of a 30 min resting-state (RS) fMRI protocol, followed by T_1 - and T_2 -weighted anatomical scans using the

MPRAGE and the SPACE sequences, respectively. An interferometric turbo-FLASH B_1^+ mapping protocol (5 mm isotropic resolution, repetition time [TR] = 20 s, acquisition time [TA] = 4 min 40 s) (Fautz et al., 2008; Brunner and Pruessmann, 2009) and multiple gradient recalled echo (GRE) protocol (2.5 mm isotropic resolution, TR = 8.4 ms, 3 echoes, echo times [TE] = 2.7, 4.2, 6 ms, TA = 30 s) were also added in order to quantitatively assess the B_1^+ and ΔB_0 distributions for each subject and each acquisition mode.

The RS-fMRI part used a 15 min fat-suppressed MB-EPI acquisition applied twice, with the in-plane phase encoding direction being flipped during the second run (AP followed by PA). Subjects were instructed to keep their eyes open and focus on a red fixation cross on a black screen. EPI acquisition parameters were: 90 axial slices of 1.6 mm thickness with no gap, standard sinc excitation (time-bandwidth product = 3.2, Hanning window apodization), nominal flip angle = 45°, TR = 1 s, voxel size = (1.6 mm)³, in plane field of view (FOV) = 208 × 208 mm, multi-band slice acceleration factor = 5 with blipped-CAIPIRINHA FOV/3 inter-slice shift, in-plane GRAPPA acceleration factor = 2 with 52 autocalibration lines (ACS) acquired separately using the fast low angle excitation echo-planar technique (FLEET) (Polimeni et al., 2016), partial Fourier acquisition = 7/8, readout bandwidth = 1832 Hz/pixel, fat saturation with nominal flip angle = 80°. Online image reconstruction was performed with the implementation of the MGH blipped-CAIPI MB-EPI C2P (www.nmr.mgh.harvard.edu/software/c2p/sms), which uses sequential application of Slice-GRAPPA (Setsompop et al., 2012) with leak-block (Cauley et al., 2014) and GRAPPA (Griswold et al., 2002).

The T_1 - and T_2 -weighted acquisitions were in sagittal orientation, isotropic resolution of 0.8 mm, FOV = 256 × 224 × 208 mm (read, phase and partition axes) and a GRAPPA acceleration factor of 2 in the phase encode direction. Other parameters were: TR = 2.6/3.0 s, MPRAGE inversion time = 1.1 s, echo spacing (ES) = 10.2/8.6 ms, readout bandwidth = 240/370 Hz/pixel, flip angle = 4°/Muglerfls approach (Mugler, 2014; Mugler et al., 2000) respectively for the MPRAGE and SPACE acquisitions.

2.2. Design of parallel transmission Universal Pulses

Dynamic RF shimming with spoke (slice-selective) and k_T -point (non-selective) pulses use a simple and low-dimensional parameterization of the RF and gradient waveforms. It consists of i) the different RF shimming weights, defined by the time integral of the RF shim sub-pulses, and ii) the transmit k-space (Cloos et al., 2012b) displacement vectors, i.e. the time integral of the interleaved magnetic field gradient blips along the three axes. In this framework, efficient non-linear constrained optimization algorithms can be applied to attempt finding the best possible dynamic RF-shimming solution (Hoyos-Idrobo et al., 2014).

The UPs used for the MB-EPI, the MPRAGE and the SPACE acquisitions in pTX were designed offline on a database $\mathcal{B}$ of measured subject-based B_1^+ and ΔB_0 maps of size $N_{\mathcal{B}} = 10$ (5 female), acquired in a separate study (Gras et al., 2017a). The UP design consisted in evaluating the subject-specific objective $\varepsilon_{\text{tailored}}$ (typically a measure of the mean deviation of the flip angle distribution across the region of interest) on every subject of the database and computing the mean objective across this database. The UP-objective ε_{UP} may thus be written as:

$$\varepsilon_{\text{UP}}(p) = \frac{1}{N_{\mathcal{B}}} \sum_{j \in \mathcal{B}} \varepsilon_{\text{tailored}}\left(\mathcal{S}_j, p\right), \tag{1}$$

where p denotes the dynamic RF shimming parameterization to be optimized, and $\varepsilon_{\text{tailored}}(\mathcal{S}_j, p)$, the evaluation of the subject-based objective on subject $\mathcal{S}_j$ of the database for the parameterization p. Hence, without any additional difficulty, hardware (RF power and gradient slew rate limits) and safety (SAR) constraints can be enforced explicitly for the UP design following exactly the same methodology used

for a subject-tailored pulse design. This was implemented using the active-set non-linear constrained optimization algorithm (Hoyos-Idrobo et al., 2014), available in the optimization toolbox of MATLAB (R2016b, the Mathworks, Natick, MA). The hardware constraints were i) the peak RF amplitude limit (170 V per TX channel at the coil plug), ii) the average RF power limit per TX channel (3 W), iii) the total average RF power limit (16 W) and iv) the maximum slew rate of the magnetic field gradient coils (200 mT/m/ms). The SAR thresholds were expressed in terms of global and local SAR limits of 3.2 W/kg and 10 W/kg respectively (International Electrotechnical Commission, 2015).

For the design of the non-selective UPs (SPACE and MPRAGE sequences), the subject-tailored objective was defined as the normalized root mean square (NRMS) deviation of the flip angle distribution $\alpha(r)$ from the target flip angle α_T, calculated across the brain (region $\mathcal{R}$), i.e.:

$$\varepsilon_{\text{tailored,3D}} = \frac{1}{|\alpha_T|} \left(\frac{1}{|\mathcal{R}|} \sum_{r \in \mathcal{R}} (\alpha(r) - \alpha_T)^2 \right)^{\frac{1}{2}}, \tag{2}$$

where $|\mathcal{R}|$ and r denote the number of brain voxels of the B_1^+ map and the spatial coordinates, respectively. For the design of the slice-selective UPs (MB-EPI sequence), the objective was formulated as a weighted NRMS deviation from the target flip angle across the brain with the slice-dependent weighting function:

$$w(r) = \exp\left(-d_0^{-1} \max\left(0, d(r, P) - \frac{\theta}{2} \right) \right) \tag{3}$$

where denotes the median plane of the considered slice, $d(r, P)$ the Euclidean distance from r to, θ the slice thickness, and $d_0 = 1$ cm. The objective in this case for a single slice thus is given by the equation:

$$\varepsilon_{\text{tailored,2D}} = \left(\frac{1}{\sum_{r \in \mathcal{R}} w(r)} \sum_{r \in \mathcal{R}} w(r) \, (\alpha(r) - \alpha_T)^2 \right)^{\frac{1}{2}}. \tag{4}$$

We note here that taking $d_0 = 0^+$ leads to the weighting function $w = 1$ for $r \in P$, which is the conventional way of designing slice-specific spokes pulses. Taking into account all voxels in $\mathcal{R}$, and letting the flip angle deviation have an (exponentially) decreasing weight as the distance from the slice of interest, promotes robustness of the pulse against variations in the slice positions and small tilts. Likewise, taking $d_0 = \infty$, leads to $w = 1$ everywhere and the 2D objective converges to the 3D objective in that case. The choice of a 1 cm soft threshold was found to offer a good compromise between excitation performance and robustness.

In equations (2) and (4), for all but the inversion pulse, the flip angle distribution $\alpha(r)$ was computed using the small tip angle approximation (Pauly et al., 1989a). This approximation provides a linear relationship between the RF weights and the flip angle (Boulant and Hoult, 2012) which is valid for up to moderate target flip angles or for symmetric pulses (Pauly et al., 1989b; Eggenschwiler et al., 2014; Gras et al., 2018). For the inversion pulse, this approximation being not valid, $\alpha(r)$ was obtained by numerical integration of Bloch's equations (Bloch integration). For the computation of $\alpha(r)$, relaxation effects during the pulse were neglected.

For the design of the MB-EPI UPs, coherent summation of the slice-specific RF pulses within each multiband slice group was assumed for simplicity to ensure that peak RF amplitude of the multiband waveforms of any slice group did not exceed the hardware peak power limit. This has a simple and tractable implementation as it involves only a reasonable number of constraints per multiband slice group (the product of the number of transmit channels by the number of spokes). For this particular scenario (8 transmit channels, two spokes and MB-5), the subsequent optimization of the global (consistent across all transmit channels and spokes) RF phase offsets between the different slices of the same multiband slice group (Wong, 2012) returned a reduction of peak amplitude of 20%.

Owing to the smooth variation of the B_1^+ field and the weighting function in the 2D objective above, RF coefficients and spokes-placement in k-space (Dupas et al., 2015) were optimized for every other slice only (45 slices among 90) and the same parametrization was attributed to the adjacent slice (Wu et al., 2013; Tse et al., 2016). To comply with the multiband acceleration (here of 5), the spoke placement optimization was done concurrently for all slices of a multiband group (the set of slices excited simultaneously). Finally, the bipolar two-spoke pulses were designed with a subpulse duration of 2180 μs and a total pulse duration of 4800 μs (excluding the slice selection rewinder). Prior to designing the bipolar spokes, the gradient delay was characterized on phantom using sub-μs precision and compensated for by manipulating the RF phase of the second spoke (Gras et al., 2017c). As shown also elsewhere (Tse et al., 2016), characterizing and correcting for this delay with such precision is a necessary ingredient for multi-bipolar spoke applications away from the iso-center. Unipolar designs, where both slice selection gradients share the same polarity, are inherently insensitive to these imperfections but they have less spectral bandwidth due to a longer duration and are more prone to peripheral nerve stimulations due to the additional gradient lobe.

The pTX UP MPRAGE acquisition used k_T-point pulses (Cloos et al., 2012b) for the 4° excitation and 180° inversion pulses, as described in ref. (Gras et al., 2017a). The excitation used 4° flip angle (800 μs total duration with 7 gradient blips of 40 μs each) while the 180° inversion pulse lasted 4000 μs (9 subpulses of 400 μs each). The sTX pulse implementation used a standard 700 μs-long square pulse for the 4° excitation and a standard 10 ms hyperbolic-secant adiabatic pulse for inversion.

The pTX UP SPACE acquisition was based on a unique scalable (Eggenschwiler et al., 2014) k_T-point pulse (9 subpulses, total duration = 1100 μs), consistently with the methodology proposed in ref. (Gras et al., 2018). The leading excitation pulse was implemented using the same k_T-point pulse, but scaled to produce a 90° flip angle and with 90° phase offset to satisfy the Carr-Purcell-Meiboom-Gill (CPMG) condition. Scalability of the refocusing pulses, was enforced by exploiting symmetries and applying a dedicated optimization routine (Gras et al., 2018). This allowed using a unique k_T-point pulse to implement the entire array of non-selective pulses of the variable flip angle TSE readout and the preceding 90° excitation. The sTX implementations of the SPACE acquisition used standard 500 μs- and 700 μs-long square pulses for the 90° excitation and the variable flip angle TSE readout respectively.

2.3. Analysis of pulse performance and additional simulations

The RF pulse performance was assessed post-hoc by performing voxel-wise Bloch simulations using the B_1^+ and B_0 offset maps that were acquired on each subject in addition to the (f)MRI scans. The CV of the flip angle and the MR signal were calculated across the brain. The interest of analyzing the signal homogeneity (as the ultimate measure of interest in practice) in addition to the flip angle (the physical parameter that drives the RF pulse optimization) is to take into account the non-linear dependence of MR signal with the flip angle. The MR signal was computed for a representative pair of T_1/T_2 values for brain white matter at 7T, namely $1300/60$ ms.

For the MB-EPI sequence, to provide a comparison of the proposed two-spoke UP design with the volume (global) (Krishnamurthy et al., 2019) and slice-specific RF shimming (Wu et al., 2019) (one-spoke pulses), additional sets of simulations were performed in which the bipolar two-spoke design was replaced with the (simpler) one-spoke design (pulse duration 4520 μs), with otherwise identical design parameters as for the 2-spoke UPs): i) a set of 45 slice-specific *universal* RF-shims using the database of B_1^+ and B_0 offset maps and the UP objective, ii) a set of 45 slice-specific and subject-tailored (Wu et al., 2019) RF-shims per subject, and iii) a global ($d_0 \rightarrow \infty$) subject-tailored RF-shim over the whole head, per subject.

The gain in robustness with respect to slice position and inclination

provided by the weighted least-squares approach (see Equation (4)) was also tested through the following simulation. The 45-slice UP design for the MB-EPI protocol was repeated with a weighted-least squares soft threshold d_0 (see Equation (3)) of 1 mm (instead of 10 mm). The coefficient of variation of the flip angle (45 slices merged together) of both sets of pulses was then computed for different values of slice position offsets (up to 20 mm) and slice inclinations (rotation about the right-left axis of up to 20°).

2.4. fMRI pre-processing and temporal SNR calculations

The MB-EPI data were first motion-corrected using FSL McFLIRT (Jenkinson et al., 2002). The two 900-volume series (with AP and PA phase encoding directions) of each session were then distortion-corrected based on FSL Topup (Andersson et al., 2003). The temporal SNR was then calculated for each voxel, subject and session by taking the mean of the corresponding time-series divided by its standard deviation, after linear de-trending and removal of the first 10 vol to reject the transient spin evolution towards steady-state from the analysis. The tSNR maps were then registered to the Montreal Neurological Imaging (MNI152) template by using the FSL FLIRT affine registration tool with 12 degrees of freedom (Jenkinson and Smith, 2001), aided by the T_1-weighted anatomical scan. This allowed computation of an average tSNR map across subjects and generation of inflated cortical surface representations by using PySurfer (https://github.com/nipy/PySurfer). In order to provide a common ground and not bias the comparison of sTX versus pTX, the same (pTX) T_1-weighted scan was used for the registration.

2.5. Analysis of the resting-state data

After motion correction, distortion correction and registration as described above, the time varying signals associated to each voxel were standardized to display a unit-variance, detrended and band-pass filtered (0.01–0.1 Hz) (Goelman et al., 2017). The 6 motion parameters (3 for translation, 3 for rotation) of the time-series realignment procedure and physiological noise related confounds were regressed out using CompCor (Behzadi et al., 2007).

Correlated BOLD fluctuations were identified using the seed-based approach, by selecting a voxel in the brain (seed) and calculating the correlation between its associated signal and all other voxel time-series. For the present analysis, the seed was a spherical volume of 8 mm in diameter located in the posterior cingulate cortex (center coordinates: $[0, -50, 26]$ on the MNI152 template). For all voxels across the brain, the Pearson correlation coefficient relative to this seed was then calculated and mapped onto inflated cortical surfaces using nilearn (Abraham et al., 2014).

In the resting brain, The BOLD signal in the posterior cingulate cortex is known to correlate with the one observed in the inferior parietal and medial prefrontal cortices as well as the temporal cortex (Raichle et al., 2001; Vincent et al., 2006), thus characterizing the so-called default mode network. The aim of this analysis hence was to reproduce this finding on a subject-by-subject basis and compare the correlation maps between acquisition modes. The hypothesis here is that a better BOLD sensitivity translates into higher correlations in this seed-based analysis of the DMN.

3. Results

3.1. Comparison of image quality

Fig. 1 provides a comparison of the MB-EPI, MPRAGE and SPACE acquisitions obtained in subjects 1 to 5 in pTX versus sTX. All sTX acquisitions display signal losses in the temporal lobes, of which one coronal section is shown in the figure. For the MB-EPI acquisition, this signal loss directly affects BOLD sensitivity as the SNR and tSNR naturally scale with the MR signal. The introduction of $CaTiO_3$ dielectric pads (second
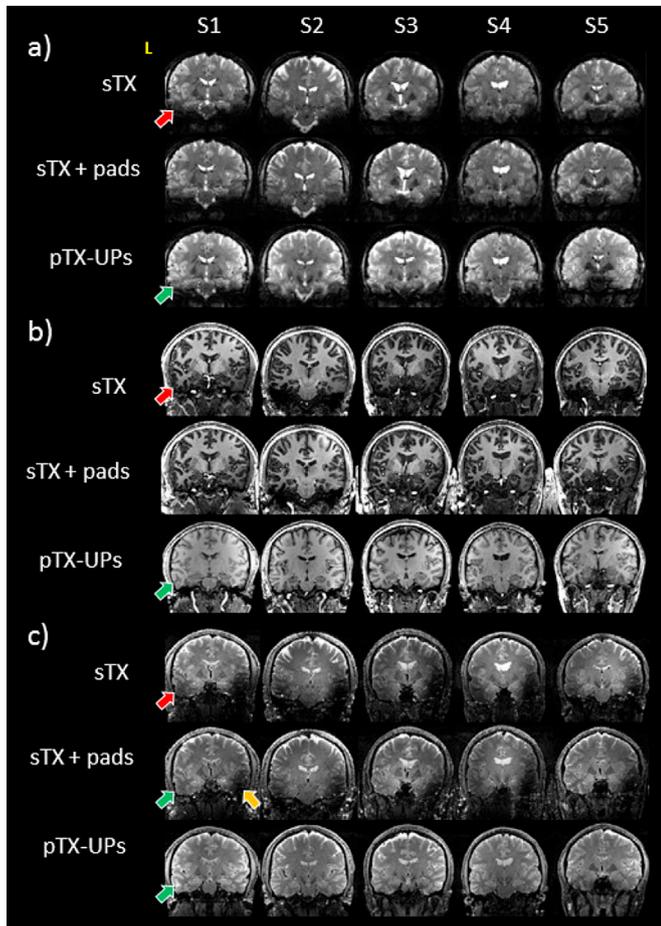
Fig. 1. Image comparison comparisons for the different acquisition modes and sequences. EPI with MB = 5 (a), b) MPRAGE and c) SPACE acquisitions obtained in subjects 1 to 5 in sTX (with and without dielectric padding) versus pTX are provided. For all subjects (S1 to S5), a marked signal loss is present in both sTX acquisitions (top and middle rows in a-c) in the temporal lobes (red arrows). For all subjects, such signal loss or contrast deterioration is absent in the pTX UP acquisitions (bottom row), as indicated by the green arrows. The dielectric pads (clearly visible in the MPRAGE and SPACE images) were able to compensate for the signal drop in all subjects, mostly in the left temporal lobe. As can be seen for instance in the SPACE acquisition of S1, the favorable influence of the dielectric pad however was clearly asymmetric as it was not able to restore a good contrast for the right temporal lobe (orange arrow).

rows in a)-c)) somewhat reduces but does not eliminate the signal loss. For the SPACE acquisition, which makes use of an optimized flip angle train to enable long TSE readouts, the flip angle heterogeneity severely degrades the signal and the contrast in lower brain regions. As confirmed by the flip angle analysis that follows, with pTX and universal k_T -point pulses, the flip angle error is reduced to a level that is sufficient to obtain T_2 -weighted 3D images free of B_1^+ artifacts. In the MPRAGE images, the improvement with UPs was less pronounced because the preservation of the gray-white matter contrast is mostly governed by the quality of the inversion preparation. In sTX, we observed that the hyperbolic-secant adiabatic inversion pulse provided good inversion efficiency over the whole brain, with the exception of a small portion of the cerebellum or the temporal lobes in some subjects. The major image imperfection that remains in the T_1 -weighted scans in sTX thus is a signal drop in regions of low B_1^+ , more detrimental to SNR than image contrast. As a general rule for MPRAGE, a smaller flip angle for the FLASH readout leads to stronger contrast, but a weaker signal (Gras et al., 2016). As a result, undershot FLASH excitations in sTX results in a stronger gray-white matter contrast, but a weaker SNR than observed in the pTX acquisitions.

3.2. Assessment of RF pulse performance by simulation

Fig. 2 provides a comparison of the functional and anatomical images that were obtained in one representative subject with the three acquisition modes (pTX UPs, sTX and sTX with dielectric pads) evaluated in this study. For the coronal plane that is displayed, the associated flip angle distribution obtained retrospectively in simulation using the RF pulse definition and the subject-specific B_1^+ and ΔB_0 maps is shown on the right side. The flip angle profile in sTX displays flip angle values ranging from 30% to 110% of the target value. Using pTX UP slice-specific two-spoke multi-band (for MB-EPI) and volume-selective k_T -point pulses (for the MPRAGE inversion and FLASH pulses, and the SPACE excitation and refocusing pulses), much greater homogeneity of the excitation profiles is achieved.

The CV of the flip angle and the MR signal for $T_1/T_2 = 1300/60$ ms across the brain (i.e. the region of interest) with respect to the mean flip angle is reported in Table 1. These were computed for the 45° slice-selective pulses of the MB-EPI acquisition, the 4° non-selective pulse used in the MPRAGE sequence and the 90° excitation pulse used in the SPACE sequence. The statistical significance of the flip angle and the signal heterogeneity reductions (pTX UP versus sTX) was also quantified using paired t-tests. For all sequences, the CV of the MR signal was statistically significant ($p < 2 \times 10^{-5}$). While the CV of the flip angle typically exceeds 25% in sTX, the UP approach allows to restore an excitation uniformity at least as good as typically seen on a clinical 3 T system (13%) with standard transmission hardware (Boulant et al., 2008). Using pTX UPs, the CV of the MB-EPI signal ranged from 4% to 6% while it always exceeded 14% using sTX. For the 3D T_1 -weighted and T_2 -weighted anatomical scans, the signal's CV was below 13% in pTX while it often exceeded 25% in sTX with and without dielectric padding. The dielectric pads were helpful in compensating for the B_1^+ drop in their vicinity (the left and right temporal lobes) but, this had a minimal impact on the CV, the latter criterion being a global performance measure.

The simulated flip angle homogeneity of the two-spoke versus the one-spoke pulse designs for the pTX-enabled MB-EPI sequence is provided in Table 2. The universal 2-spoke design (the one evaluated experimentally in this work) is comparable in performance with the tailored 1-spoke design ($p = 0.8$), applied in another study (Wu et al., 2019). This raises the question whether a 1-spoke universal design, simpler than the 2-spoke universal design, would be sufficient. In simulation, the 1-spoke UP design indeed yields a significantly better signal CV than the sTX acquisition (5–8% versus 14–17%, $p = 0.047$), but a poorer homogeneity as compared to the two-spoke universal or 1-spoke tailored design (3–6%). Hence for one subject, the flip angle CV exceeds 16%, that is, a signal uniformity that is superior to that observed on a clinical 3 T system (Boulant et al., 2008). The subject-specific global RF shim on the other hand returned flip angle CVs of 17% up to 20%.

The robustness of the multiband UPs with respect to a shift in the slice positions or an inclination of the slices is showed in Fig. 3. As expected, the set of pules obtained with the 1 cm soft-threshold perform better than the other with respect to a variation in the position or the inclination of the slice. Note that $d_0 = 1$ mm practically leads to no weighting since the spatial resolution of the B_1^+ maps is 5 mm. This result also indicates that the tolerance of the universal MB-EPI pulses designed in this study can be considered as high as 2 cm for the slice position offset and 20° for the slice inclination. Indeed, for both cases, the CV in flip angle does not exceed 13%.

3.3. Temporal SNR

Projections of the tSNR maps onto cortical surfaces for each subject are shown in Fig. 4. In each subject, tSNR of the pTX UP scans exceeds that of the sTX acquisitions, without and with pads), which is consistent with the flip angle simulations reported above. Additionally, a comparison of the average (across the five subjects after normalization to the
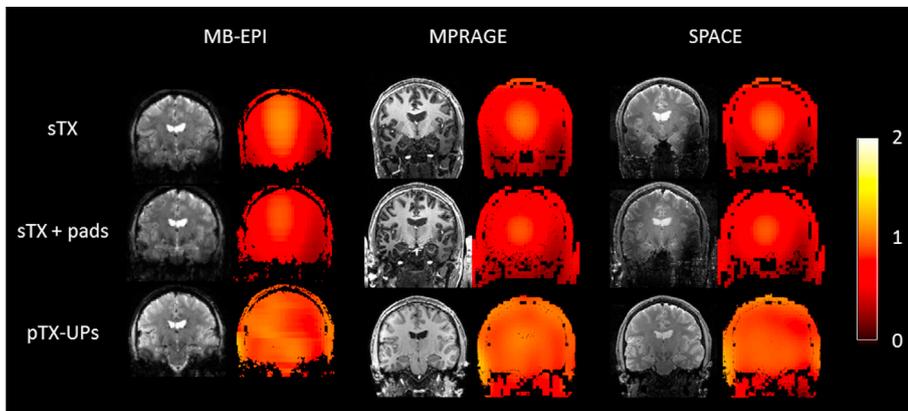
Fig. 2. Coronal views for one representative subject of the MB-EPI, MPRAGE and SPACE images with corresponding simulated flip angle simulations. For every scan, the underlying flip angle distribution (obtained by retrospective simulation from the measured subject-specific B_1^+ and ΔB_0 distribution) is displayed in units of the nominal FA distribution. Even in the presence of dielectric pads, the sTX acquisition mode displays a strong flip angle heterogeneity, with values ranging from 30% up to 110% the nominal flip angle (respectively the 1%- and the 99%-quantiles of the flip angle distribution in the brain). This heterogeneity is largely removed in the pTX-UP acquisition mode.

Table 1
CV (in percent) of the flip angle (FA) and the MR signal (best case − worst case over 5 subjects) for the MB-EPI, the MPRAGE and the SPACE HCP-style protocols at 7T. For the sTX acquisition mode, relative homogeneity is consistent for all sequence types given that pulses involved in those sequences do not use the dynamic RF shimming principle. The values displayed in parenthesis are p-values of statistical paired t-tests performed on the signal NRMS deviation between the pTX UP acquisitions and the sTX acquisitions.

	pTX UPs		sTX		sTX + pads	
	FA	Signal	FA	Signal	FA	Signal
MB-EPI	9–11	4–6	22–24	15-17 (2.10^{-5})	20–22	14-17 (8.10^{-5})
MPRAGE	7–9	8–10	”	22-25 (7.10^{-6})	”	21-23 (3.10^{-6})
SPACE	8–11	9–13	”	34-40 (3.10^{-5})	”	35-41 (4.10^{-6})

Table 2
NRMS deviation (in percent) of the flip angle (FA) and the MR signal (best case − worst case over 5 subjects) for the slice-specific universal 2-spoke, tailored slice-specific (s.s.) and global RF shims, and universal 1-spoke pulse designs. Using universal 2-spoke pulses, the signal NRMS deviation is significantly lower than with universal 1-spoke pulses ($p = 0.047$). The same comparison with tailored 1-spoke pulses yet gives $p = 0.8$, i.e. no statistical evidence that the universal 2-spoke design outperforms the tailored 1-spoke design.

objective	#spokes	FA	Signal
universal	2	9–11	4–6
	1	12–16	5-8 ($p = 0.047$)
tailored s.s.	1	9–12	3-5 ($p = 0.8$)
tailored global	1	17–20	6-8 ($p = 0.005$)

MNI152 template) temporal SNR maps is displayed in Fig. 5a. A marked tSNR gain with pTX can be seen, in particular in the temporal, occipital and parietal lobes, where the transmit efficiency of the RF coil in sTX is weaker. This is also demonstrated by the ratio maps (Fig. 5b) which reveal tSNR gains of up to 100% between the pTX and the sTX acquisitions. On average across all subjects and over the whole brain, the tSNR gain using UPs amounted to 25%.

In this study, we used a different, standard, (pre) processing pipeline (FSL for realignment and distortion correction, nilearn for normalization and denoising) than the one defined in the HCP protocol (Van Essen et al., 2013), and in which the T_2-weighted scan was not employed for registration and segmentation. However, for the HCP data analysis framework, the contrast uniformity enhancement enabled by UPs for the T_2-weighted acquisition (see Fig. 1) could be beneficial to improve the quality of the segmentation. In this study, We found for instance that the registration to the MNI template using FSL (with default processing parameters) was more robust if the pTX-rather than the sTX-MPRAGE acquisition was selected as the input anatomical image. We shall note however that a more thorough and expert use of the software could have improved the robustness of the registration with the sTX-MPRAGE acquisition.

3.4. Resting-state analysis

Fig. 6 reports the seed-based analysis of the DMN performed on all subjects and for all setups. Here, stronger time-correlations between the posterior cingulate cortex and the temporal cortex can be seen in the data acquired with pTX UPs. This observation is consistent with the reported tSNR increase in the same regions. However, due to the small number of subjects involved in this study, no statistical analysis of the increased time-correlation was performed. It is also interesting to note a more pronounced left-right symmetry in the pTX UP results, which conforms to the description of the DMN as a symmetric network in the literature (Smith et al., 2009).

4. Discussion

Parallel transmission has long been advocated as promising technology to tackle standing wave effects at UHF, and enormous progress has been made in the past decade. But to date, the cumbersome operation and need for time-consuming calibrations typically result in these precious resources to be underused in actual application studies. The UP approach circumvents these limitations as it allows for a scanner operation that is no different from a sTX exam. A parallel here can be drawn with another proposed plug and play pTX approach (Cloos et al., 2016), which yet relies on the MR fingerprinting (MRF) concept. The major philosophical difference from UP lies in how the RF field inhomogeneity is dealt with: UPs tackle it at the excitation stage whereas the plug and play MRF technique resolves it at the reconstruction stage by disentangling its effects from the rest of the data. While the latter has shown promising results for quantitative MRI, it is yet not clear how the same framework could be leveraged to fMRI. The UP concept on the other hand is theoretically compatible with any type of MRI acquisition.

As shown in a previous work (Gras et al., 2017b), slightly superior pTX excitation performance can be achieved with full subject-specific RF pulse calibrations (Gras et al., 2017b). Another price to pay with UPs is the increased SAR and power demands engendered by their broadband behavior to be robust versus the variability of the B_0 offset across subjects (Gras et al., 2017b). The MB-EPI bipolar spoke UPs implemented in this work saturated the peak 10 g SAR of our VOP model (safety factor of 2.3) as well as the peak and total average power constraints, while the MPRAGE and SPACE acquisitions still left a factor of around 2 in TR to manoeuvre with. Considering the integration of pTX into a clinical setting, however, the incremental performance gain of subject-tailored pulses would probably not outweigh the additional effort of calibrating B_1^+, performing computationally expensive online pulse calculation and
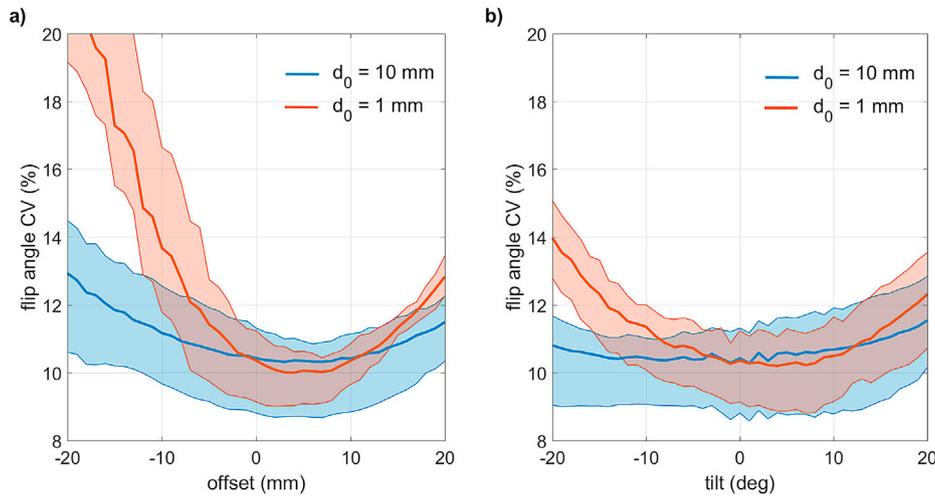
Fig. 3. Simulation of the flip angle CV (45 slices pooled together) as a function of a) the slice shift and b) the slice inclination (about the right-left axis) for the universal pentaband pulses designed with a weighted least-squares parameter d_0 (see Equation (3)) of 1 mm (red curve) and 1 cm (the proposed design parameter, blue curve). For each plot, the thick line and the two enclosing lines represent the mean, the minimum and the maximum of the CV across the five subjects.
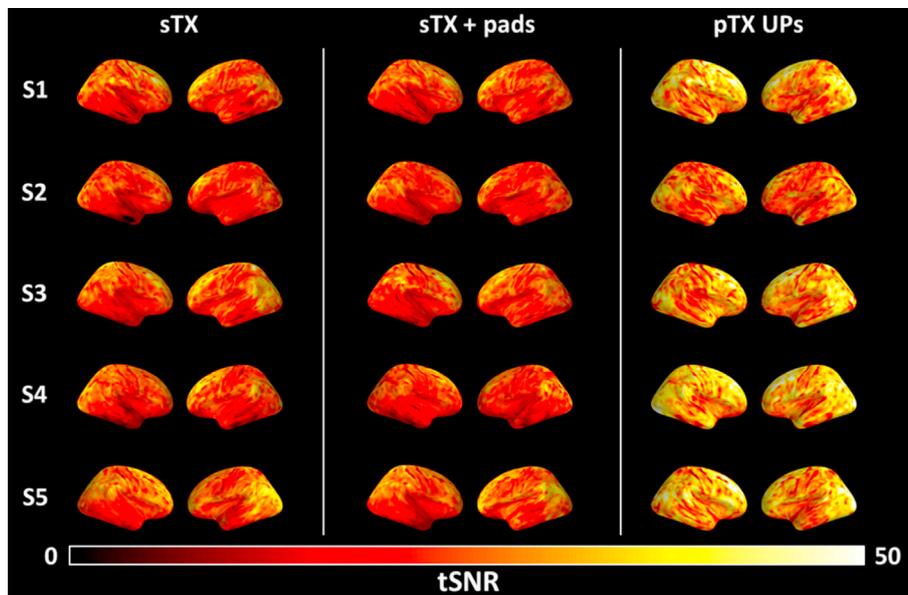

Fig. 4. Cortical surface projection of the tSNR maps obtained for the left and right hemispheres for subjects 1 to 5 (top to bottom) and for the three different setups (left to right). Using pTX and UPs, a higher tSNR can be achieved over the cortex consistently throughout all subjects.

other complex pTX-related steps. As an indication of the time that would be needed to perform the calculations (any other operation than the pure pulse optimization taken aside) for this specific protocol in pTX with subject-tailored pulses (slice-specific RF shimming for the MB-EPI sequence and same k_T-point parameterization as for the UPs for the MPRAGE and SPACE sequences), the RF pulse computation times on a DELL Precision 7510 (processor Intel Core i7-6820HQ, 16 Gb of RAM) were 10 s, 48 s and 104 s for the MB-EPI, the MPRAGE and the SPACE sequences respectively. These times were returned for 100 iterations of our optimization algorithm (active-set) and 4 initial random k-space trajectories (for the k_T-points), which is an acceptable trade-off between performance and computation time, yet in our experience with low chances to return the global optimum. In addition, the subject-specific approach is prone to errors from any imprecision of the B_1^+ measurement, which is a particular risk in rapid B_1^+ mapping (Pohmann et al., 2016). Finally, the subject-specific approach relies on B_0 offset and B_1^+ maps that are typically obtained once at the beginning of the examination, and so any subsequent patient motion will impose further errors.

The UP approach effectively removes this risk and provides robust universally applicable dynamic RF shims that are pre-calculated from a set of high-quality calibration data. Interestingly also, the use of UPs provides an additional layer of RF safety in that they can be extensively validated with prior phantom scans (e.g. by temperature mapping). Session-specific subject-tailored RF pulses, as they do not exist until the actual scan occurs, do not allow such extensive RF safety tests and so their compliance with the IEC guidelines can only be assessed by means of numerical SAR simulations (the ones giving rise to the VOP model).

In this work, plug and play pTX acquisitions were characterized for the specific example of the HCP-style 7T whole-brain resting-state fMRI protocol, by an excitation uniformity of significantly lower CVs than in standard sTX operation without and with dielectric pads. The excitation uniformity of the slice-selective and non-selective UPs that enable plug-and-play pTX were in fact comparable to the B_1^+ uniformity of a volume coil at 3 T, where RF field inhomogeneity in the brain is not considered obstructive to clinical use. We furthermore verified experimentally that the improvement in the excitation uniformity translated
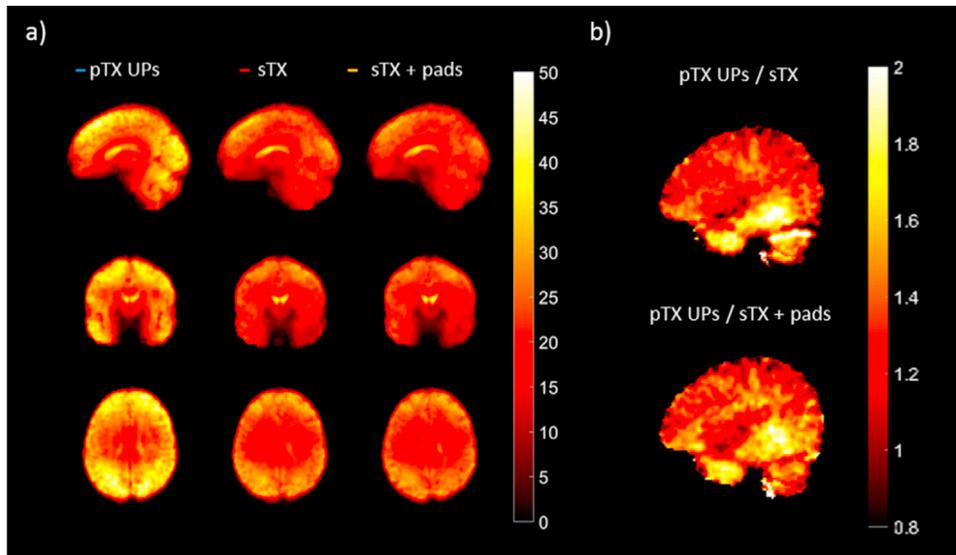
Fig. 5. Average tSNR data. a) Three-plane view of the average (across all five subjects) tSNR map for the pTX UP (left column), in sTX (middle column) and sTX with dielectric pads (right column) acquisitions. Averaging was performed after normalization to the MNI152 standard space. b) tSNR ratio maps of pTX/sTX and pTX/sTX with pads shown for one sagittal slice through the right temporal lobe, showing a considerable tSNR enhancement in that region for the UP approach.

into a gain in tSNR and in a more robust measurement and analysis of the signal correlations in the resting brain. This is illustrated by the seed-based DMN result (Fig. 6) which displayed stronger correlations with the use of pTX UPs than in sTX. One may naturally expect that this sensitivity gain translates directly to task-based fMRI.

For the MB-EPI acquisition, as shown in 2, we found in flip angle simulations that the proposed UP two-spoke design was comparable in performance with the subject-tailored slice-specific RF shimming (one-spoke design) that was recently proposed in HCP-style RS-fMRI scans at 7T (Wu et al., 2019), and outperformed the subject-tailored volume RF shimming approach. Moving to a one-spoke slice-specific UP on the other hand resulted in significantly impaired excitation quality and robustness across subjects. Here, one subject had a flip angle CV above 16% for the UP RF shimming scenario. As a result, the key advantage of using the UP technique for conducting HCP-style RS-fMRI experiments at 7T is that it combines the excitation performance typical of subject-tailored slice-specific RF shimming for SMS-EPI with the simplicity of use of sTX. While the first requirement is important to fully exploit the SNR and sensitivity gain at high field, the second is fundamental for the pTX technology to be embraced by new potential users. In the following, we mention some of the limitations that one should be aware of before switching to pTX UPs, and propose directions to mitigate them.

Adopting the proposed plug-and-play pTX framework can impose some restrictions on the protocol preparation, in particular for the MB-EPI case. Indeed, for the 2D case, since the two-spoke UP parameters (spokes RF amplitudes and locations in the transmit k-space) are optimized for a fixed slice position, these slice positions, in principle, cannot be modified for the acquisition. To mitigate this, we have proposed a weighted least-squares optimization procedure that promotes some robustness with respect to slice placement. This strategy not only gives a tolerance with respect to the actual position of the slices, but also some tolerance in the slice inclination. As a consequence, it also promotes robustness in terms of flip angle stability in case of motion. Furthermore, by increasing the value of the soft-threshold d_0 (in this study, it was set to 1 cm), it is possible to select a desired degree of robustness, naturally at the expense of performance in the ideal setting. Note here that the MPRAGE and SPACE acquisitions, as well as any 3D sequence, using non-selective dynamic RF shimming pulses, do not have this limitation at all. Hence, for those acquisitions, the position and orientation of the field of view can be set arbitrarily.

The fact that the design of UP is dependent of the flip angle that is targeted can appear as another obstacle, in particular if the latter parameter is supposed to be varied across experiments. We shall note however that the MB-EPI spokes pulses being designed by using the small tip angle approximation, reasonably valid up to 90° (Boulant and Hoult, 2012), different flip angles can be targeted by simply scaling the RF waveforms of the pulses. The repetition time of the sequence can be changed as long as the RF power and SAR limits are fulfilled. Just as in sTX acquisitions, the pulse duration likewise can be adjusted to accommodate these constraints, without having to recalculate the pulses, yet with increased penalty with respect to B_0 robustness. To provide more optimal solutions, different sets of pulses with different energy loads but identical duration could also be designed. The small tip angle and refocusing pulses in the MPRAGE and SPACE sequences being scalable as well, the same reasoning holds for the 3D anatomical scans.

The fact that the UP framework requires the adoption of bipolar 2-spoke pulses to preserve the same quality of excitation as the subject-tailored slice-specific RF shim does not impose a significant penalty in terms of the time-efficiency of the pulse, since the only excitation time overhead amounts to twice the ramp duration of the slice selection gradient. However, a limitation of the current implementation, and which does not exist for 1-spoke pulses, is that the slices could not be tilted (although this functionality can be desirable in practice, e.g. to maximize brain coverage with a minimum number of slices). This limitation is due to the way the gradient delay correction was performed, namely the application of a slice-dependent RF phase offset to the second spoke RF pulse (Gras et al., 2017c). This strategy unfortunately does not allow slice tilting unless the gradient delay is the same for the *x*, *y* and *z* gradient coils. This however can be overcome in future work by adopting a more general correction strategy which consists in encoding the gradient delay correction in the second spoke k-space location rather than in the second spoke RF phase, by using so-called trim-blips (Oelhafen et al., 2004).

5. Conclusions

Calibration-free pTX was successfully implemented in the entire HCP RS-fMRI protocol at 7T, including anatomical scans, by means of slice-specific bipolar two-spoke SMS-UPs (MB = 5) and non-selective k_T point UPs. The flip angle homogeneity reported in this study with universal slice-specific two-spoke MB-EPI pulses (9–11% across 5 subjects) is comparable to the flip angle homogeneity obtained with subject-tailored

Figure 6. Radar plots of the time-correlation coefficient between the posterior cingulate cortex (seed) and the DMN-associated left parietal, the right parietal, the left temporal, the right temporal and the frontal regions for the five subjects (S1-S5) and the three acquisition modes (sTX, sTX + pads and pTX). Although below significance level due to the small number of subjects involved in this study, this result strongly suggests that higher levels of correlation can be seen in the pTX acquisition mode, in particular in the left and right temporal regions.

slice-specific RF shim pulses. With this work, we report for the first time a plug and play utilization of a multi-transmit multi-receive RF coil for whole-brain BOLD fMRI at ultra-high field which, for MB-EPI, gives access to the same quality of excitation as subject-tailored slice-specific RF shimming without deviating from simple routine scanning. As compared with the single transmission mode, with and without dielectric pads, a noticeable gain in tSNR (up to 2-fold in B_1^+ deprived regions) resulting into a higher sensitivity for the BOLD-induced neural activity, and an improved contrast uniformity in whole-brain anatomical scans were reported.

Conflicts of interest

CEA has filed provisional patent applications directed to this technology.

Acknowledgements

References

Abraham, A., Pedregosa, F., Eickenberg, M., Gervais, P., Mueller, A., Kossaifi, J., Gramfort, A., Thirion, B., Varoquaux, G., 2014. Machine learning for neuroimaging with scikit-learn. Front. Neuroinf. 8. http://journal.frontiersin.org/article/10.33 89/fninf.2014.00014/abstract. ISSN 1662–5196.

Andersson, J.L., Skare, S., Ashburner, J., Oct. 2003. How to correct susceptibility distortions in spin-echo echo-planar images: application to diffusion tensor imaging. Neuroimage 20 (2), 870–888. http://linkinghub.elsevier.com/retrieve/pii/S1 053811903003367. ISSN 10538119.

Behzadi, Y., Restom, K., Liau, J., Liu, T.T., 2007. A component based noise correction method (CompCor) for BOLD and perfusion based fMRI. Neuroimage 37 (1), 90–101.

Beqiri, A., Hoogduin, H., Sbrizzi, A., Hajnal, J.V., Malik, S.J., 2018. Whole-brain 3D FLAIR at 7T using direct signal control. Magn. Reson. Med. 0 (0). https://onlinelibrar y.wiley.com/doi/abs/10.1002/mrm.27149. ISSN 1522–2594.

Boulant, N., Hoult, D.I., 2012. High tip angle approximation based on a modified BlochRiccati equation. Magn. Reson. Med. 67 (2), 339–343. https://doi.org/ 10.1002/mrm.23270. ISSN 1522–2594.

Boulant, N., Le Bihan, D., Amadon, A., 2008. Strongly modulating pulses: a new method for tackling RF inhomogeneity problems at high fields. Magn. Reson. Med. 68, 701–708.

Boulant, N., Gras, V., Amadon, A., Ferrand, G., Vignaud, A., 2018. Workflow proposal for defining SAR safety margins in parallel transmission. In: Proceedings of the 26th Annual Meeting of ISMRM, Page Abstract 295, Paris.

Brunner, D.O., Pruessmann, K.P., 2009. B1+ interferometry for the calibration of RF transmitter arrays. Magn. Reson. Med. 61 (6), 1480–1488. https://doi.org/10.1002/ mrm.21893. ISSN 1522–2594.

Cauley, S.F., Polimeni, J.R., Bhat, H., Wald, L.L., Setsompop, K., July 2014. Interslice leakage artifact reduction technique for simultaneous multislice acquisitions. Magn. Reson. Med. 72 (1), 93–102. https://onlinelibrary.wiley.com/doi/abs/10.1002/mr m.24898. ISSN 1522–2594.

Cloos, M.A., Boulant, N., Luong, M., Ferrand, G., Giacomini, E., Hang, M.-F., Wiggins, C.J., Bihan, D.L., Amadon, A., 2012a. Parallel-transmission-enabled magnetization-prepared rapid gradient-echo T1-weighted imaging of the human brain at 7T. Neuroimage 62 (3), 2140–2150. http://www.sciencedirect.com/science/article/pii/ S1053811912005563. ISSN 1053–8119.

Cloos, M.A., Boulant, N., Luong, M., Ferrand, G., Giacomini, E., Le Bihan, D., Amadon, A., 2012b. kT-points: short three-dimensional tailored RF pulses for flip-angle homogenization over an extended volume. Magn. Reson. Med. 67 (1), 72–80. https:// doi.org/10.1002/mrm.22978. ISSN 1522–2594.

Cloos, M.A., Knoll, F., Zhao, T., Block, K.T., Bruno, M., Wiggins, G.C., Sodickson, D.K., Aug. 2016. Multiparametric imaging with heterogeneous radiofrequency fields. Nat. Commun. 7, 12445. https://www.nature.com/articles/ncomms12445. ISSN 2041–1723.

Dupas, L., Massire, A., Amadon, A., Vignaud, A., Boulant, N., 2015. Two-spoke placement optimization under explicit specific absorption rate and power constraints in parallel transmission at ultra-high field. J. Magn. Reson. 255 (0), 59–67. http://www.scienc edirect.com/science/article/pii/S1090780715000750. ISSN 1090–7807.

Eggenschwiler, F., O'Brien, K.R., Gruetter, R., Marques, J.P., 2014. Improving T2-weighted imaging at high field through the use of kT-points. Magn. Reson. Med. 71 (4), 1478–1488. https://doi.org/10.1002/mrm.24805. ISSN 1522–2594.

Eichfelder, G., Gebhardt, M., 2011. Local specific absorption rate control for parallel transmission by virtual observation points. Magn. Reson. Med. 66 (5), 1468–1476. https://doi.org/10.1002/mrm.22927. ISSN 1522–2594.

Fautz, H.-P., Vogel, M., Gross, P., Kerr, A., Zhu, Y., 2008. B1 mapping of coil arrays for parallel transmission. In: Proceedings of the 16th Annual Meeting of ISMRM, p. 1247.

Garrec, M., Gras, V., Hang, M.-F., Ferrand, G., Luong, M., Boulant, N., 2016. Probabilistic analysis of the specific absorption rate intersubject variability safety factor in parallel transmission MRI. Magn. Reson. Med. 78 (3), 1217–1223. https://onlinelibrary. wiley.com/doi/abs/10.1002/mrm.26468.

Glasser, M.F., Sotiropoulos, S.N., Wilson, J.A., Coalson, T.S., Fischl, B., Andersson, J.L., Xu, J., Jbabdi, S., Webster, M., Polimeni, J.R., Essen, D.C.V., Jenkinson, M., 2013. The minimal preprocessing pipelines for the Human Connectome Project. Neuroimage 80, 105–124. http://www.sciencedirect.com/science/article/pii/S1053811913005053. Mapping the Connectome. ISSN 1053–8119.

Goelman, G., Dan, R., Rika, F., Bezdicek, O., Rika, E., Roth, J., Vymazal, J., Jech, R., Mar. 2017. Frequency-phase analysis of resting-state functional MRI. Sci. Rep. 7, 43743. http://www.nature.com/articles/srep43743. ISSN 2045–2322.

Gras, V., Vignaud, A., Mauconduit, F., Luong, M., Amadon, A., Le Bihan, D., Boulant, N., 2016. Signal-domain optimization metrics for MPRAGE RF pulse design in parallel transmission at 7Tesla: signal-Domain Optimization Metrics for MPRAGE RF Pulse Design. Magn. Reson. Med. 76, 1431–1442. http://doi.wiley.com/10.1002/mrm.26043. ISSN 07403194.

Gras, V., Boland, M., Vignaud, A., Ferrand, G., Amadon, A., Mauconduit, F., Bihan, D.L., Stöcker, T., Boulant, N., 2017a. Homogeneous non-selective and slice-selective parallel-transmit excitations at 7Tesla with universal pulses: a validation study on two commercial RF coils. PLoS One 12 (8), e0183562. http://journals.plos.org/plosone/article?id=10.1371/journal.pone.0183562. ISSN 1932–6203.

Gras, V., Vignaud, A., Amadon, A., Le Bihan, D., Boulant, N., 2017b. Universal pulses: a new concept for calibration-free parallel transmission. Magn. Reson. Med. 77, 635–643. https://doi.org/10.1002/mrm.26148. ISSN 1522–2594.

Gras, V., Vignaud, A., Amadon, A., Mauconduit, F., Le Bihan, D., Boulant, N., Jan. 2017c. New method to characterize and correct with sub-s precision gradient delays in bipolar multispoke RF pulses. Magn. Reson. Med. 78, 2194–2202. http://onlinelibrary.wiley.com/doi/10.1002/mrm.26614/abstract. ISSN 1522–2594.

Gras, V., Mauconduit, F., Vignaud, A., Amadon, A., Le Bihan, D., Stöcker, T., Boulant, N., July 2018. Design of universal parallel-transmit refocusing k_t-point pulses and application to 3D T_2-weighted imaging at 7T: universal Pulse Design of 3d Refocusing Pulses. Magn. Reson. Med. 80 (1), 53–65. http://doi.wiley.com/10.1002/mrm.27001. ISSN 07403194.

Grissom, W., Yip, C.-y., Zhang, Z., Stenger, V.A., Fessler, J.A., Noll, D.C., 2006. Spatial domain method for the design of RF pulses in multicoil parallel excitation. Magn. Reson. Med. 56 (3), 620–629. https://doi.org/10.1002/mrm.20978. ISSN 1522–2594.

Griswold, M.A., Jakob, P.M., Heidemann, R.M., Nittka, M., Jellus, V., Wang, J., Kiefer, B., Haase, A., June 2002. Generalized autocalibrating partially parallel acquisitions (GRAPPA). Magn. Reson. Med. 47 (6), 1202–1210. http://doi.wiley.com/10.1002/mrm.10171. ISSN 0740–3194.

Gumbrecht, R., Oct. 2013. Development of Customized pTx MR Excitation Methods and Their Safe Application. PhD thesis. Friedrich-Alexander-Universität Erlangen-Nürnberg, Erlangen.

Hoyos-Idrobo, A., Weiss, P., Massire, A., Amadon, A., Boulant, N., Mar. 2014. On variant strategies to solve the magnitude least squares optimization problem in parallel transmission pulse design and under strict SAR and power constraints. IEEE Trans. Med. Imaging 33 (3), 739–748. https://doi.org/10.1109/TMI.2013.2295465. ISSN 0278–0062.

International Electrotechnical Commission, 2015. IEC 60601-2-33 Medical Electrical Equipment - Part 2-33: Particular Requirements for the Basic Safety and Essential Performance, 3.2 edition. ISSN 978–2–8322–2743-5.

Jenkinson, M., Smith, S., June 2001. A global optimisation method for robust affine registration of brain images. Med. Image Anal. 5 (2), 143–156. http://www.sciencedirect.com/science/article/pii/S1361841501000366. ISSN 1361–8415.

Jenkinson, M., Bannister, P., Brady, M., Smith, S., Oct. 2002. Improved optimization for the robust and accurate linear registration and motion correction of brain images. Neuroimage 17 (2), 825–841. http://linkinghub.elsevier.com/retrieve/pii/S1053811902911328. ISSN 10538119.

Katscher, U., Börnert, P., Leussler, C., van den Brink, J.S., 2003. Transmit SENSE. Magn. Reson. Med. 49 (1), 144–150. https://doi.org/10.1002/mrm.10353. ISSN 1522–2594.

Krishnamurthy, N., Santini, T., Wood, S., Kim, J., Zhao, T., Aizenstein, H.J., Ibrahim, T.S., Jan. 2019. Computational and experimental evaluation of the Tic-Tac-Toe RF coil for 7Tesla MRI. PLoS One 14 (1), e0209663. https://journals.plos.org/plosone/article?id=10.1371/journal.pone.0209663. ISSN 1932–6203.

Massire, A., Vignaud, A., Robert, B., Le Bihan, D., Boulant, N., Amadon, A., 2015. Parallel-transmission-enabled three-dimensional T2-weighted imaging of the human brain at 7Tesla. Magn. Reson. Med. 73, 2195–2203. https://doi.org/10.1002/mrm.25353. ISSN 1522–2594.

Moeller, S., Yacoub, E., Olman, C.A., Auerbach, E., Strupp, J., Harel, N., Uğurbil, K., May 2010. Multiband multislice GE-EPI at 7Tesla, with 16-fold acceleration using partial parallel imaging with application to high spatial and temporal whole-brain fMRI. Magn. Reson. Med. 63 (5), 1144–1153. http://onlinelibrary.wiley.com/doi/10.1002/mrm.22361/abstract. ISSN 1522–2594.

Mugler, J.P., Apr. 2014. Optimized three-dimensional fast-spin-echo MRI. J. Magn. Reson. Imaging 39 (4), 745–767. http://onlinelibrary.wiley.com/doi/10.1002/jmri.24542/abstract. ISSN 1522–2586.

Mugler, J.P., Brookeman, J.R., 1990. Three-dimensional magnetization-prepared rapid gradient-echo imaging (3d MP RAGE). Magn. Reson. Med. 15, 152–157.

Mugler, J.P., Kiefer, B., Brookeman, J.R., 2000. Three-dimensional T2-weighted imaging of the brain using very long spin-echo trains. In: Proceedings of the 8th Annual Meeting of ISMRM, p. 687.

Oelhafen, M., Pruessmann, K.P., Kozerke, S., Boesiger, P., Nov. 2004. Calibration of echo-planar 2D-selective RF excitation pulses. Magn. Reson. Med. 52 (5), 1136–1145. http://doi.wiley.com/10.1002/mrm.20248. ISSN 0740–3194.

Padormo, F., Beqiri, A., Hajnal, J.V., Malik, S.J., Sept. 2016. Parallel transmission for ultrahighfield imaging. NMR Biomed. 29 (9), 1145–1161. https://www.ncbi.nlm.nih.gov/pmc/articles/PMC4995736/. ISSN 0952–3480.

Pauly, J., Nishimura, D., Macovski, A., 1989a. A k-space analysis of small-tip-angle excitation. J. Magn. Reson. 81 (1), 43–56. http://www.sciencedirect.com/science/article/pii/0022236489902655. ISSN 0022–2364.

Pauly, J., Nishimura, D., Macovski, A., 1989b. A linear class of large-tip-angle selective excitation pulses. J. Magn. Reson. 82 (3), 571–587. http://www.sciencedirect.com/science/article/pii/0022236489902199. ISSN 0022–2364.

Pohmann, R., Speck, O., Scheffler, K., 2016. Signal-to-noise ratio and MR tissue parameters in human brain imaging at 3, 7, and 9.4 tesla using current receive coil arrays. Magn. Reson. Med. 75 (2), 801–809. https://doi.org/10.1002/mrm.25677. ISSN 1522–2594.

Polimeni, J.R., Bhat, H., Witzel, T., Benner, T., Feiweier, T., Inati, S.J., Renvall, V., Heberlein, K., Wald, L.L., Feb. 2016. Reducing sensitivity losses due to respiration and motion in accelerated Echo Planar Imaging by reordering the auto-calibration data acquisition. Magn. Reson. Med. 75 (2), 665–679. https://www.ncbi.nlm.nih.gov/pmc/articles/PMC4580494/. ISSN 0740–3194.

Raichle, M.E., MacLeod, A.M., Snyder, A.Z., Powers, W.J., Gusnard, D.A., Shulman, G.L., 2001. A default mode of brain function. Proc. Natl. Acad. Sci. Unit. States Am. 98 (2), 676–682.

Saekho, S., Yip, C.-y., Noll, D.C., Boada, F.E., Stenger, V.A., 2006. Fast-kz three-dimensional tailored radiofrequency pulse for reduced B1 inhomogeneity. Magn. Reson. Med. 55 (4), 719–724. https://doi.org/10.1002/mrm.20840. ISSN 1522–2594.

Setsompop, K., Alagappan, V., Gagoski, B., Witzel, T., Polimeni, J., Potthast, A., Hebrank, F., Fontius, U., Schmitt, F., Wald, L.L., Adalsteinsson, E., 2008. Slice-selective RF pulses for in vivo B1+ inhomogeneity mitigation at 7Tesla using parallel RF excitation with a 16-element coil. Magn. Reson. Med. 60 (6), 1422–1432. https://doi.org/10.1002/mrm.21739, 1522–2594.

Setsompop, K., Gagoski, B.A., Polimeni, J.R., Witzel, T., Wedeen, V.J., Wald, L.L., May 2012. Blipped-controlled aliasing in parallel imaging for simultaneous multislice echo planar imaging with reduced g-factor penalty. Magn. Reson. Med. 67 (5), 1210–1224. https://onlinelibrary.wiley.com/doi/abs/10.1002/mrm.23097. ISSN 1522–2594.

Smith, S.M., Fox, P.T., Miller, K.L., Glahn, D.C., Fox, P.M., Mackay, C.E., Filippini, N., Watkins, K.E., Toro, R., Laird, A.R., Beckmann, C.F., Aug. 2009. Correspondence of the brain's functional architecture during activation and rest. Proc. Natl. Acad. Sci. U. S. A. 106 (31), 13040–13045. https://www.ncbi.nlm.nih.gov/pmc/articles/PMC2722273/. ISSN 0027–8424.

Tse, D.H., Wiggins, C.J., Poser, B.A., 2016. Estimating and eliminating the excitation errors in bipolar gradient composite excitations caused by radiofrequency-gradient delay: example of bipolar spokes pulses in parallel transmission. Magn. Reson. Med. 78 (5), 1883–1890. https://onlinelibrary.wiley.com/doi/abs/10.1002/mrm.26586.

Uğurbil, K., Xu, J., Auerbach, E.J., Moeller, S., Vu, A.T., Duarte-Carvajalino, J.M., Lenglet, C., Wu, X., Schmitter, S., de Moortele, P.F.V., Strupp, J., Sapiro, G., Martino, F.D., Wang, D., Harel, N., Garwood, M., Chen, L., Feinberg, D.A., Smith, S.M., Miller, K.L., Sotiropoulos, S.N., Jbabdi, S., Andersson, J.L., Behrens, T.E., Glasser, M.F., Essen, D.C.V., Yacoub, E., 2013. Pushing spatial and temporal resolution for functional and diffusion MRI in the Human Connectome Project. Neuroimage 80, 80–104. http://www.sciencedirect.com/science/article/pii/S1053811913005065. Mapping the Connectome. ISSN 1053–8119.

Van Essen, D.C., Smith, S.M., Barch, D.M., Behrens, T.E.J., Yacoub, E., Uğurbil, K., Oct. 2013. The Wu-minn human connectome Project: an overview. Neuroimage 80, 62–79. http://www.sciencedirect.com/science/article/pii/S1053811913005351. ISSN 1053–8119.

Vincent, J.L., Snyder, A.Z., Fox, M.D., Shannon, B.J., Andrews, J.R., Raichle, M.E., Buckner, R.L., Dec. 2006. Coherent spontaneous activity identifies a hippocampal-parietal memory network. J. Neurophysiol. 96 (6), 3517–3531. http://www.physiology.org/doi/10.1152/jn.00048.2006. ISSN 0022–3077.

Vu, A.T., Jamison, K., Glasser, M.F., Smith, S.M., Coalson, T., Moeller, S., Auerbach, E.J., Uğurbil, K., Yacoub, E., 2017. Tradeoffs in pushing the spatial resolution of fMRI for the 7T Human Connectome Project. Neuroimage 154, 23–32. http://www.sciencedirect.com/science/article/pii/S1053811916306681. ISSN 1053–8119.

Webb, A., July 2011. Dielectric materials in magnetic resonance. Concepts Magn. Reson. 38A (4), 148–184. http://doi.wiley.com/10.1002/cmr.a.20219. ISSN 15466086.

Wong, E., 2012. Optimized phase schedules for minimizing peak RF power in simultaneous multi-slice RF excitation pulses. In: Proceedings of the 20th Annual Meeting of ISMRM, p. 2209.

Wu, X., Schmitter, S., Auerbach, E.J., Moeller, S., Uğurbil, K., Van de Moortele, P.-F., Sept. 2013. Simultaneous multislice multiband parallel radiofrequency excitation with independent slice-specific transmit B1 homogenization: simultaneous Multislice Parallel RF Excitation. Magn. Reson. Med. 70 (3), 630–638. http://doi.wiley.com/10.1002/mrm.24828. ISSN 07403194.

Wu, X., Auerbach, E.J., Vu, A.T., Moeller, S., Lenglet, C., Schmitter, S., Van de Moortele, P.-F., Yacoub, E., Uğurbil, K., 2018. High-resolution whole-brain diffusion mri at 7T using radiofrequency parallel transmission. Magn. Reson. Med. 80 (5), 1857–1870. https://onlinelibrary.wiley.com/doi/abs/10.1002/mrm.27189. ISSN

Wu, X., Auerbach, E.J., Vu, A.T., Moeller, S., Van de Moortele, P.-F., Yacoub, E., Uğurbil, K., Jan. 2019. Human Connectome Project-style resting-state functional MRI at 7Tesla using radiofrequency parallel transmission. Neuroimage 184, 396–408. http://www.sciencedirect.com/science/article/pii/S1053811918308231. ISSN 1053–8119.

Yacoub, E., Shmuel, A., Pfeuffer, J., Van De Moortele, P.-F., Adriany, G., Andersen, P., Vaughan, J.T., Merkle, H., Uğurbil, K., Hu, X., Mar. 2001. Imaging brain function in humans at 7Tesla. Magn. Reson. Med. 45 (4), 588–594. https://onlinelibrary.wiley.com/doi/abs/10.1002/mrm.1080. ISSN 0740–3194.

Zhu, Y., 2004. Parallel excitation with an array of transmit coils. Magn. Reson. Med. 51 (4), 775–784. http://onlinelibrary.wiley.com/doi/10.1002/mrm.20011/full.